Dynamics of a Molecular Glass Former: Energy Landscapes for Diffusion in Ortho-Terphenyl

S. P. Niblett,[1, a)] V. K. de Souza,[1, b)] J. D. Stevenson,[1] and D. J. Wales[1, c)]

University Chemical Laboratories, Lensfield Road, Cambridge CB2 1EW, UK

Relaxation times and transport processes of many glass-forming supercooled liquids exhibit a super-Arrhenius temperature dependence. We examine this phenomenon by computer simulation of the Lewis-Wahnström model for ortho-terphenyl. We propose a microscopic definition for a single-molecule cage-breaking transition and show that, when correlation behaviour is taken into account, these rearrangements are sufficient to reproduce the correct translational diffusion constants over an intermediate temperature range in the supercooled regime. We show that super-Arrhenius behaviour can be attributed to increasing negative correlation in particle movement at lower temperatures, and relate this to the cage-breaking description. Finally, we sample the potential energy landscape of the model, and show that it displays hierarchical ordering. Substructures in the landscape, which may correspond to metabasins, have boundaries defined by cage-breaking transitions. The cage-breaking formulation provides a direct link between the potential energy landscape and macroscopic diffusion behaviour.

[a)] sn402@cam.ac.uk

[b)] vkd21@cam.ac.uk

[c)] dw34@cam.ac.uk

I. INTRODUCTION

A glass former is a liquid that may be supercooled below its melting point without crystallisation.[1–3] At a temperature T_g the relaxation time exceeds the experimental timescale and the system falls out of equilibrium, becoming mechanically solid but retaining an amorphous, liquid-like, structure. This is the kinetic glass transition. Investigation of this transition remains one of the most active areas of research in statistical physics,[3–7] partly because glass-forming behaviour is displayed by a wide range of liquids when cooled sufficiently quickly.[1,2,8] The use of glasses in industrial and everyday applications is similarly widespread, providing further motivation.[3,9] A major objective for theoretical work in this field is to identify the mechanism of the dynamical slowdown,[3,4,7,10] which is key to understanding the transition but which has not been convincingly attributed to a structural change on cooling.

The phenomenon of super-Arrhenius behaviour is a particularly active area of study.[11–16] Dynamic processes are usually associated with relaxation across a single energy barrier, so they obey the Arrhenius law, and the corresponding transport coefficients (e.g. diffusion constants and viscosity) scale with temperature according to $e^{\pm B/T}$, where B is constant. However for many glass formers (termed "fragile")[17,18] a stronger "super-Arrhenius" temperature dependence is observed in the supercooled regime.

Previously, the super-Arrhenius behaviour of the binary Lennard-Jones fluid (BLJ) was shown to arise from a quantifiable negative correlation in particle motion, which increases at lower temperatures.[19,20] These negative correlations were interpreted in terms of a microscopic definition for cage-breaking processes[21] and the connectivity of the potential energy landscape.[22] In the present contribution, the cage-breaking definition is extended to molecular systems, so that a similar analysis can be applied to a coarse-grained model for ortho-terphenyl. This rigid body system is a more representative model than BLJ for molecular fragile glass formers.

In section II the model system and molecular dynamics simulation details are presented. The trajectories obtained from these simulations are then analysed in terms of cage-breaking (section III) and short-time diffusion (section IV). Finally, the trajectories are used as starting points to examine the potential energy landscape (PEL) directly, in section V.

II. METHODS

A. Model

Ortho-terphenyl (1,2-diphenylbenzene, OTP) is a well-known fragile glass former, which has been extensively studied experimentally[23–25] and by simulation.[26–28] It is reported that the melting temperature $T_M = 328\,\mathrm{K}$, and the glass transition temperature $T_g \approx 243\,\mathrm{K}$.[25]

Some simulations treat OTP almost completely atomistically,[26] but it is common to rigidify much of the molecule to reduce the complexity of the simulation.[27–30] The most popular coarse-grained model is that of Lewis and Wahnström,[31–34] which describes OTP as an isosceles triangle of sites with fixed bond lengths and fixed unique angle 75°. Each site interacts pairwise additively with all sites in other molecules according to the Lennard-Jones potential, which is commonly used to model non-directional dispersion forces such as those that dominate intermolecular interactions for OTP. The bond lengths are set to σ, the Lennard-Jones distance unit.

The model used here retains the Lewis-Wahnström geometry, but adds a Stoddard-Ford quadratic cutoff[35] to the potential, so that both the energy and its distance derivative go smoothly to zero at the cutoff. This property is required for landscape analysis because gradient discontinuities cause unstable behaviour in geometry optimisation.[8]

The complete potential for each site-site interaction is:

$$\begin{gathered} V_2(r) = 4\epsilon\left[\left(\tfrac{\sigma}{r}\right)^{12} - \left(\tfrac{\sigma}{r}\right)^{6}\right] + \lambda_1 + \lambda_2 r^2, \\ \lambda_1 = 4\epsilon\left[-7\left(\tfrac{\sigma}{r_c}\right)^{12} + 4\left(\tfrac{\sigma}{r_c}\right)^{6}\right],\ \lambda_2 = \tfrac{4\epsilon}{r_c^2}\left[6\left(\tfrac{\sigma}{r_c}\right)^{12} - 3\left(\tfrac{\sigma}{r_c}\right)^{6}\right], \end{gathered} \tag{1}$$

where r_c is the cutoff distance. The well depth of the modified potential, ϵ_0, depends weakly on r_c. Following Mossa *et al.*[32] we chose $r_c = 2.614\,\sigma$, which gives $\epsilon_0 = -0.9570\,\epsilon$.

The original study of the Lewis-Wahnström model employed $\epsilon_0 = 600\,k_B\,\mathrm{K} = 4.988\,\mathrm{kJ\,mol^{-1}}$ and $\sigma = 0.483\,\mathrm{nm}$ to fit the molar volume and diffusion constant against experiment at 400 K.[31] In the present work, the energy scale was chosen such that the modified well depth ϵ_0 corresponds to the same energy. Thus, the energy unit $\epsilon = 5.209\,\mathrm{kJ\,mol^{-1}}$.

T/K	ρ/g cm^{-3}	Production Time/ns
260	1.082	369.04
266	1.079	268.39
275	1.076	100.65
291	1.065	33.549
305	1.055	33.549
346	1.027	33.549

TABLE I. Input parameters for the MD trajectories as a function of temperature. The equilibration time of 10^6 steps (16.7 ns) is excluded.

B. Molecular Dynamics Simulation

To provide dynamical data for the diffusion study and an initial set of configurations from which to sample the PEL, canonical MD simulations of bulk OTP were performed at a range of temperatures. The propagator used to solve the equations of motion employs quaternions to describe the orientation of the rigid particles.[36] The algorithm combines an explicit symplectic integrator with the Nosé-Poincaré thermostat. The timestep was 16.7 fs. Temperatures were studied in the range 260 K to 346 K.

The simulation consisted of 324 OTP molecules in a cubic box with periodic boundary conditions. The molar volume was varied (see table I) to correspond with the original study of Lewis and Wahnström.[31] This system size was large enough to reproduce literature values for the diffusion constants but small enough to mitigate some of the problems associated with landscape analysis of large systems. In particular, identifying rearrangements that correspond to single-particle processes is harder when the system is large enough to contain multiple non-interacting sub-systems. The system size chosen here is a compromise between minimising finite-size effects and multiple-subsystem effects.

10^6 MD steps were allowed for equilibration from a simple cubic starting structure. Subsequently, configurations of the trajectory were saved every 100 steps (1.67 ps). The simulation length was varied with temperature (table I) to allow the colder trajectories to reach local ergodicity, which was diagnosed using the Mountain-Thirumalai energy fluctuation metric[18,37] and the non-Gaussian parameter for translational displacement.[19,38]

In much of the analysis which follows, we make use of inherent structures: local potential energy minima whose basins of attraction are explored by the trajectory. At high and very low temperatures the energies of these inherent structures are independent of

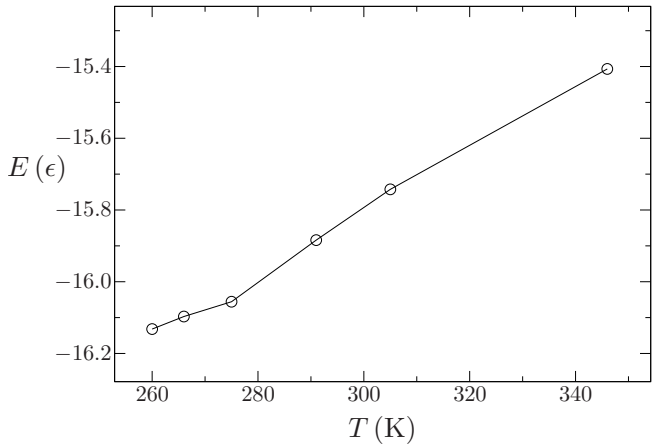

FIG. 1. Inherent structure energies per particle for OTP MD trajectories at different temperatures.

temperature, but for a particular range of supercooled temperatures the energies decrease with system temperature.[39] This behaviour defines the "landscape-influenced" temperature regime.[1] Fig. 1 presents the energies of inherent structures sampled by our trajectories, showing the general decrease associated with the landscape-influenced region, but beginning to level off into the landscape-dominated regime at low temperatures. For comparison, we calculated the energy of the bcc-like crystal structure of the Lewis-Wahnström model[40] at the ideal density of $1.2537\,\mathrm{g\,cm^{-1}}$ assuming perfect orientational ordering. We found this energy to be $-17.839\,\epsilon = -92.979\,\mathrm{kJ\,mol^{-1}}$.

III. CAGE-BREAKING ANALYSIS

Simulations of fragile glass formers well below their freezing temperature reveal that, between short-time ballistic motion and long-time diffusive behaviour, there exists an intermediate time regime where the mean-square displacement of a particle is effectively constant.[41] This observation corresponds to trapping of particles in a cage of their nearest neighbours, restricting their mobility.

Signatures of this cage effect have been identified using three-time correlation functions in hard sphere simulations,[42,43] and fabrication of hard sphere-like colloidal suspensions has allowed direct observation of cage dynamics by confocal microscopy.[44,45] The cage effect has been used in several different ways to probe the dynamics of supercooled liquids.

Caging is an important concept in the mode-coupling theory of supercooled dynamics

(MCT), where it explains the plateau region in the intermediate scattering function at low temperatures.[8,46] As the temperature is decreased, the cages become more persistent and motion between them becomes less frequent. MCT predicts a divergence of relaxation time at a critical temperature T_c where all particles become caged on an infinitely long time scale and translational diffusion halts.[8,46] In fact, values of T_c fitted from theoretical predictions significantly overestimate the observed glass transition temperature T_g. For OTP, $T_c \approx 290\,\mathrm{K}$[47] and $T_g = 243\,\mathrm{K}$[24] have been reported experimentally. This discrepancy arises because conventional MCT excludes some particle exchanges, sometimes referred to as "hopping processes".[8]

Simulations of model glasses indicate a separation of the dynamics in the deeply supercooled regime into non-diffusive "cage rattling motions" and diffusive "cage-breaking" rearrangements,[48,49] which involve changes to the nearest-neighbour environment of the central particle. Middleton and Wales showed that these two types of motion have systematically different potential energy barriers.[50]

Rabani *et al.* developed a "cage correlation function" based on changes in the nearest neighbours for a particular atom, to estimate the typical residence time within a given configuration of cages.[51,52] This function was used to reproduce non-exponential relaxation behaviour for fragile glass formers.[53,54]

There have also been a number of attempts to extend the cage concept by identifying single-particle rearrangements that involve transitions between cages. One approach is to partition the trajectory of each particle into diffusive and vibrational components,[55] while other methods involve defining cage escape events when a particle executes a jump that is large relative to the magnitude of its fluctuations on short timescales.[56,57] For example, the Debye-Waller factor has been used to approximate the magnitude of fluctuation expected for a caged particle.[49] An important observation from these studies is that many cage-changing motions are rapidly reversed, and the proportion of reversals increases with decreasing temperature.[56]

de Souza and Wales proposed a microscopic definition of a local cage-breaking process for the binary Lennard-Jones fluid.[21] In a cage-breaking transition, one or more atoms move between nearest-neighbour cages. They found that at low temperatures, the diffusion constant obtained from an MD trajectory can be approximated using only atomic displacements resulting from productive (non-reversed) cage-breaking transitions, indicating that

these transitions are the most important transport processes involved in long-time diffusion. At lower temperatures, rearrangements that cross the high energy barriers associated with cage-breaking transitions become less common. Additionally, at lower temperatures the caging particles rearrange more slowly following an escape of the central particle. This effect increases the probability of an immediate reversal of the cage break. Since productive cage breaks dominate the diffusion constant, reduced frequency of cage breaks and increased reversal probability increases the effective energy barrier to diffusion and leads to super-Arrhenius behaviour.[56]

In the present contribution we extend the cage-breaking analysis to molecular systems and demonstrate the wider relevance of the energy landscape approach by analysing OTP, a typical molecular glass former.

To analyse diffusion using the cage-breaking picture, the MD trajectories described in section II B are first transformed to "inherent trajectories".[58] Every configuration in the trajectory is quenched to a local minimum on the potential energy landscape by performing local energy minimisation with the LBFGS algorithm.[59–61] The quenching process converts the molecular dynamics trajectory into a discrete series of jumps between local minima of the PEL, removing vibrational motion and helping us to define the nearest-neighbour cage for each molecule.

This separation of dynamics into vibrational and landscape components is less appropriate at high temperatures, where the system has sufficient kinetic energy to sample configurations further from the corresponding local minimum. Hence the present work is concerned mostly with moderately supercooled temperatures, where the particles are confined to potential energy basins on much longer timescales.

Once a geometrical definition of a cage-breaking process has been established, each jump between minima in the inherent trajectory may be classified as either cage-breaking or non-cage-breaking for each molecule. If diffusion is limited by cage-breaking processes then long-time diffusion constants should be reproducible from the mean squared displacement calculated only from transitions in the inherent trajectory that correspond to cage breaks.[21]

The objective of the cage-breaking method is to identify which inherent structure transitions correspond to genuine structural rearrangements, as opposed to minor adjustments in particle positions. By focussing on elementary transitions between local minima, we identify the smallest non-local motions of the system that are relevant to long-term diffusion.

A. Defining a Cage Break

Since cages are composed of the nearest neighbours for each molecule, the definition of a cage-breaking process must involve changes in these nearest neighbours. Correctly identifying the neighbours is therefore an important step.

For BLJ, the nearest-neighbours of an atom were defined as all atoms that lie closer than a parameter r_{NN}. A suitable value of r_{NN} was chosen near the first minimum in the radial distribution function (RDF) for each type of interaction (AA,AB,BB).[21] Since the RDF has a small value either side of this cutoff, the nearest-neighbour shell is well defined.

We found that making an analogous definition for neighbours of an OTP molecule using a cutoff in the centre of mass (CoM) displacement between two molecules was not as successful. The CoM-CoM RDF, fig. 2, is less sharply peaked than the AB RDF in BLJ.[21] Hence the nearest-neighbour shell is difficult to define using this metric: any value of r_{NN} will misidentify some neighbours and fail to identify others. However, the nearest-neighbour shell of an individual site in the OTP molecule is much easier to define (since the site-site RDF, fig. 3, is more strongly peaked). Consequently, we have adopted a new definition for molecular cage breaks. The neighbours of each site in the OTP molecule are recorded separately, and cage breaks are identified for every site, following a rule similar to that used with BLJ. A molecular cage break (CB) is diagnosed only when all of the constituent sites undergo cage breaks simultaneously.

The rule used to identify CBs for individual sites ("site-CBs") differs slightly from that employed for BLJ. Instead of the fixed global cutoff distance r_{NN}, we used the solid angle nearest neighbour (SANN) method of van Meel *et al.*[62] to identify the nearest neighbours of a site within the OTP molecule. This is a parameter-free local cutoff method, with the advantage that neighbour shells defined this way should be more robust against small fluctuations in particle position, which should not be identified as neighbour changes. In the BLJ definition, such small fluctuations were dealt with using a "displacement cutoff": to register as a nearest neighbour change, the distance between the central site and its newly lost/gained neighbour had to change by at least d_c. However, for OTP it was found that the number of CBs identified depended quite strongly on the value of d_c. To eliminate another system-dependent parameter, and help make the definition of the molecular cage break more general, we omit the displacement cutoff. This change is partly compensated by the use of

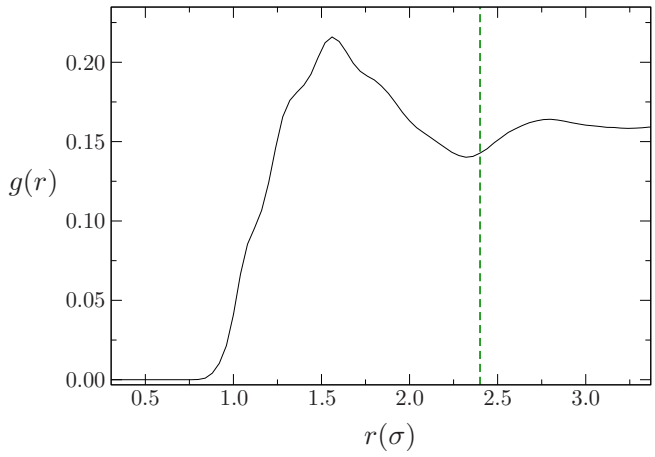

FIG. 2. The centre of mass radial distribution function for OTP. The dashed vertical line indicates a possible cutoff distance to define nearest neighbours, but the function is still significantly non-zero at this point. Therefore the centre of mass distance between molecules is not sufficient to define a nearest-neighbour shell.

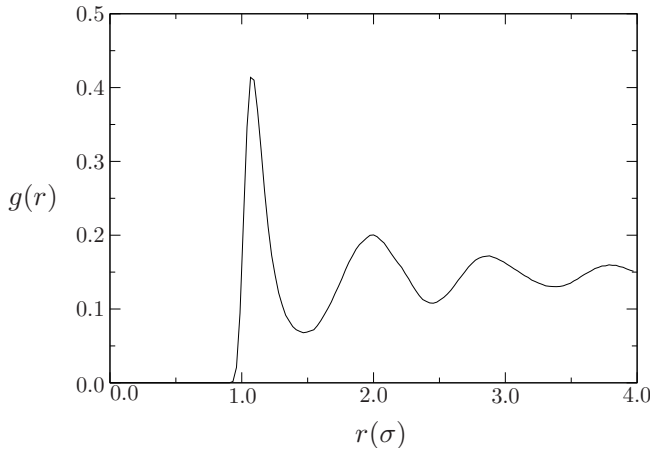

FIG. 3. The site-site radial distribution function of OTP. This is more sharply peaked than fig. 2, indicating that nearest neighbours for individual sites within the OTP molecule are easier to define.

the SANN method, and partly by the requirement for three separate site-CBs to occur for each molecular CB, which should limit the effect of local fluctuations. However, it seems likely that omitting the movement cutoff will lead to a modest overidentification of cage breaks.

Having eliminated two of the parameters that were required to define a CB in BLJ, only one remains in the definition for OTP: the number of neighbours that must change in order for a site cage break to take place. For BLJ this parameter was chosen to be two.[21] Because

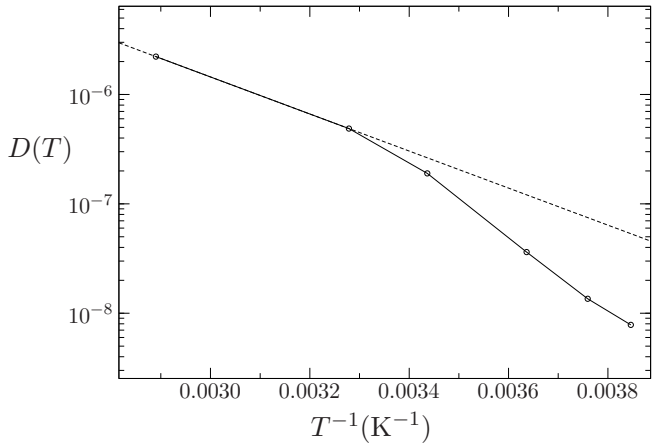

FIG. 4. Translational diffusion constants $D(T)$ for OTP, showing the deviation from hypothetical Arrhenius behaviour (demonstrated by the dashed line, which does not represent any data but is merely intended to guide the eye).

the average number of neighbours per molecule is broadly similar for BLJ and OTP, we again require two neighbours to be lost or two gained in order to define the site-CB.

An approximate diffusion constant can now be calculated using only the displacements resulting from CB transitions in the inherent trajectory, and compared with the results from the original MD trajectory.

B. Diffusion Constants

The isotropic translational diffusion of OTP was analysed by computing the diffusion constant using the Einstein equation:

$$D = \lim_{t\to\infty} \frac{1}{6t} \left\langle \mathbf{r}_i(t)^2 \right\rangle , \tag{2}$$

where $\mathbf{r}_i(t)$ is the centre-of-mass displacement at time t of particle i from its position at time 0. $\langle \ldots \rangle$ represents an average over particles and time origins.

The diffusion constants calculated from our MD trajectories using eq. (2) are presented in fig. 4. These data show super-Arrhenius behaviour, curving downwards below the dashed line, which indicates the straight-line behaviour expected for Arrhenius temperature dependence.

Cage-breaking diffusion constants were also calculated, considering only the particle mo-

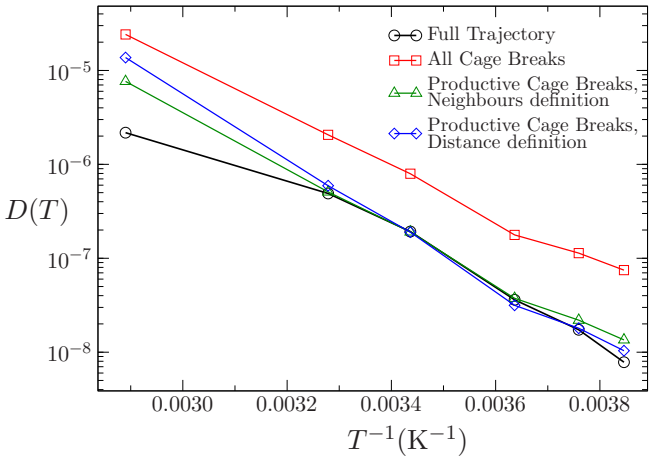

FIG. 5. Diffusion constants computed from inherent structure trajectories, taking into account only the squared displacements corresponding to cage breaks. The values calculated from the complete MD trajectory are given for comparison. Effective diffusion constants are calculated using all cage breaks and using productive cage breaks only (i.e. excluding reversed cage breaks). Two different methods for identifying reversed cage breaks are shown. Both give a much better approximation to the full-trajectory values than the all-cage-breaks results. The Distance method for identifying reversals gives a better fit than the Neighbours method, but includes a system-dependent parameter. Using productive cage breaks to approximate the full trajectory is quite accurate in the central temperature range.

tions that correspond to cage breaks. Eq. (2) is used again, but the real-time configurations from the MD trajectories are replaced by frames from the inherent structure trajectories, and the square displacement $\mathbf{r}_i(t)^2$ for molecule i is replaced by a sum of the square displacements of every CB transition of molecule i up to time t. This modification neglects all correlation in displacement direction between the CB steps.

The line in fig. 5 corresponding to effective diffusion constants calculated from all CB transitions yields a substantial overestimate of the true full-trajectory values. This result can be largely corrected by accounting for negative correlations in step direction. We approximate the required correction by discounting all molecular CBs that are subsequently completely reversed, because these rearrangements do not contribute to long-time diffusion.

There are two possible types of reversal motion: direct reversals where a molecule returns to its original cage via a second CB, and indirect reversals where the return step is by a non-CB transition. For BLJ, the first type of reversal was identified when the total squared displacement for a particular particle after two consecutive CBs was less than a threshold distance of $10^{-5}\,\sigma$.[21] The second type was identified when the displacement in two

consecutive CBs was identical to within $10^{-5}\,\sigma$.

This method, based on square displacements of consecutive cage breaks and thus termed the Distance method, fails to detect many reversals in the OTP trajectories. This is because cages in OTP are larger and more open than in BLJ due to the anisotropy of the particles. Larger cages mean that a reversed CB could leave a molecule in an equivalent nearest-neighbour environment while still being a considerable distance from its original position. Hence using an arbitrary small threshold distance, as for BLJ, fails to capture most reversal events. We followed two approaches. Firstly, we continued to use the Distance method, but gradually increased the threshold distance until a histogram showing the correlation angles of consecutive productive CBs (cf. fig. 4 in de Souza and Wales, 2008)[21] indicated that all direct reversals had been identified. This gave a value for the distance cutoff of $0.3\,\sigma$. The resulting effective diffusion constants are shown in fig. 5.

To avoid the problem of choosing a system-dependent threshold distance, we also used a second method to identify reversed CBs based on changes to the nearest-neighbour lists. Recall from section III A that we require each site in the molecule to lose or gain two nearest neighbours in a transition if that transition is to be counted as a CB. If a site-neighbour is lost in one CB and gained in the next, this neighbour change has been reversed directly. If the same neighbour is lost in two consecutive CBs, the neighbour change has been reversed indirectly. If the number of neighbours gained/lost in the first CB is less than two after discounting reversed neighbour changes, then the first CB is considered to have been reversed by the second (either directly or indirectly, according to the nature of the reversals). Note that the first CB is still considered to have taken place (since it meets the required number of site-neighbour changes) but is treated differently because it is subsequently reversed. We refer to this approach as the the Neighbours method of identifying reversals.

"Productive" cage breaks were identified for both reversal methods. We first construct a time-ordered list of all CBs for each molecule over the course of the trajectory. Each list is checked for pairs of consecutive transitions that qualify as a reversal under the above definitions. Whenever such a reversal pair is identified, both CBs are removed from the list, so that no CB transition can belong to two reversal pairs. Indirectly-reversed CBs are also removed. The remaining transitions are described as productive CBs.

Effective diffusion constants were calculated by summing the squared displacements of productive cage-breaking transitions only. These effective diffusion constants are shown in

fig. 5 for both reversal methods, along with the diffusion constants for the full (continuous) trajectory and for all cage-breaking transitions. Both productive-only lines give a dramatic improvement over the all-CBs line, fitting the full-trajectory values very well in the middle temperature range which loosely corresponds to the central part of the landscape-influenced regime. This result indicates that productive CBs (which could be defined by either method) are sufficient to describe translational diffusion in this temperature range. In both cases, the gradient of the productive-CB line is more negative than that of the all-CB line. This difference indicates that reversed CBs become more common at lower temperatures, resulting in a higher effective energy barrier to diffusion, as expected.

However, both sets of productive-CB diffusion constants badly overestimate the correct values at high temperatures, and the Neighbour method in particular gives a significant overestimate at low temperatures. Moreover, none of the cage-breaking lines shows significant super-Arrhenius curvature, which shows they are not capturing all the details of translational diffusion. This lack of super-Arrhenius curvature will be discussed further in section IV, but here we recognise that it limits the applicability of the cage-breaking description to the temperature range over which the effective diffusion constants match those obtained by MD simulation.

The error at higher temperatures is probably because the inherent structure description on which the CB method is based breaks down. The original MD trajectory wanders further from the corresponding local minima, and consequently quenching has a greater effect on the displacement between consecutive frames. So the inherent structures no longer provide a good description of diffusion.

The errors at low temperatures suggest that we are missing some negative correlation effects, perhaps indicating the existence of another type of reversal motion that we have not taken into account, for example reversals that take place via several CBs rather than a single pair of consecutive CB events. The fact that the Distance method appears to work better than the Neighbours method at lower temperatures may be insightful. Unlike the Distance method, the Neighbours method depends upon the positions of multiple molecules: both the molecule that is actually moving and all of its nearest neighbours. It is possible that the decreased frequency of CBs at low temperatures results in the Neighbours method missing some reversals, because in the time that elapses between the first and second CB in a reversal pair, the nearest neighbours may move and alter the local environment. So a

molecule could execute two cage breaks with a very small net displacement (not contributing to long-term diffusion), but still have a different list of nearest neighbours from its starting position and thus not be detected as a reversal by the Neighbours method. Missing reversals in this way becomes more likely when we consider translational-rotational decoupling, which some authors have suggested increases the rate of rotational motion relative to translational motion at low temperatures.[33,63] This decoupling would encourage changes in the cage structure on a faster timescale than that of the cage breaks themselves, which would affect the Neighbours definition of reversals but not the Distance definition.

In spite of this slight advantage of the Distance method, we will use the Neighbours definition for the remainder of this paper. We make this choice to present a general definition of productive cage breaks, which can be used for simple molecular systems without needing to choose a system-dependent parameter. Fig. 5 demonstrates that molecular rearrangements corresponding to productive CBs are a good representation of the dominant processes in translational diffusion in OTP in the central part of the landscape-influenced regime. It also demonstrates the importance of negatively correlated motion, here described by reversed cage breaks, to describe the diffusion of OTP. This negative correlation is the subject of the next section.

IV. TIME SCALE ANALYSIS OF DIFFUSION

We will now show that super-Arrhenius behaviour in OTP can be explained by considering correlation effects in the original MD trajectory, without quenching to the inherent structures. This method investigates the effect of the observation timescale on the apparent diffusion constants, retrieving the diffusion constants by arbitrary coarse-graining of the trajectory, rather than the directed coarse-graining of the cage-breaking method, where we attempt to select only the important rearrangement events.

As for BLJ,[18–20] the long (locally ergodic) MD trajectories were divided into a series of short non-ergodic intervals of length τ. The reduced diffusion constant $D(\tau)$ was calculated using eq. (2), but replacing the mean squared displacement $\langle \mathbf{r}_i(t)^2 \rangle$ with

$$\langle \mathbf{r}_i(t,\tau)^2 \rangle = \left\langle \sum_{j=1}^{m} \Delta \mathbf{r}_i(j)^2 \right\rangle, \tag{3}$$

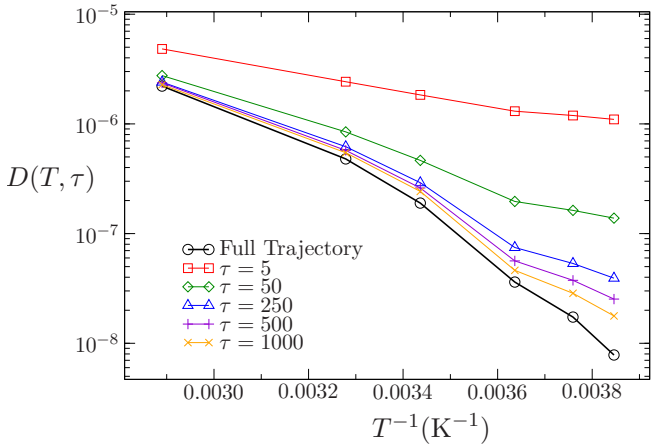

FIG. 6. Short-time apparent diffusion constants $D(T,\tau)$. Results for several values of the interval length τ are shown, along with the data from the complete trajectory in fig. 4. τ is given in MD time units, $t_{int} = 1.68\,\mathrm{ps}$. The shortest intervals give approximately Arrhenius temperature dependence, indicating that super-Arrhenius behaviour arises from correlation between particle displacements in different time intervals. As τ is increased and the intervals approach the length of the entire trajectory, the apparent diffusion constants give a better approximation to the full-trajectory values and super-Arrhenius behaviour is restored.

where $t = m\tau$ and $\Delta\mathbf{r}_i(j) = \mathbf{r}_i(j\tau) - \mathbf{r}_i((j-1)\tau)$. j indexes the time intervals.

The approximation in eq. (3) means that mean square displacements are evaluated over each interval of length τ, with the square displacement at longer times being approximated by adding together the square displacements computed over these short intervals. The resulting apparent diffusion constants are presented in fig. 6. The computed $D(\tau)$ values show roughly Arrhenius temperature dependence at small values of τ, but super-Arrhenius curvature reappears as τ increases, becoming more pronounced for large τ as the interval length approaches local ergodicity and $D(\tau)$ tends towards the values for the full trajectory.

If the effective diffusion constants show Arrhenius temperature dependence on short timescales, then the super-Arrhenius behaviour observed for the long-time $D(T)$ must be caused by the neglected terms in the approximation represented by eq. (3), namely the correlations in particle motion between the different time intervals. These correlations may be quantified by expressing the true displacement $\mathbf{r}_i(t)$ of particle i at time $t = m\tau$ in terms of the short-time displacements $\Delta\mathbf{r}_i(j)$:

$$\mathbf{r}_i(t) = \sum_{j=1}^{m} \Delta\mathbf{r}_i(j), \text{ so}$$

$$\begin{aligned}
\mathbf{r}_i(t)^2 &= \left(\sum_{j=1}^{m} \Delta\mathbf{r}_i(j)\right) \cdot \left(\sum_{k=1}^{m} \Delta\mathbf{r}_i(k)\right) \\
&= \sum_{j=1}^{m} \Delta\mathbf{r}_i(j)^2 + 2\sum_{j=1}^{m}\sum_{k=j+1}^{m} \Delta\mathbf{r}_i(j) \cdot \Delta\mathbf{r}_i(k) \\
&= \sum_{j=1}^{m} \Delta\mathbf{r}_i(j)^2 + 2\sum_{j=1}^{m}\sum_{k=j+1}^{m} \Delta r_i(j)\Delta r_i(k)\cos\theta_{jk}. \qquad (4)
\end{aligned}$$

θ_{jk} is the angle between the displacement vectors in intervals j and k, and $\Delta r_i(j)$ represents the magnitude of $\Delta\mathbf{r}_i(j)$.

Identifying the first term of eq. (4) with eq. (3), it is clear that the short-time diffusion constants $D(\tau)$ neglect the correlation terms in $\cos\theta_{jk}$. To confirm this result, an approximate correlation term may be reintroduced in $\langle\mathbf{r}_i(t,\tau)^2\rangle$ to recover the full super-Arrhenius behaviour.[19]

The average of $\cos\theta_{jk}$ over all particles and time intervals is denoted by $\langle\cos\theta_{jk}\rangle$. Fig. 7 shows this quantity as a function of the number of time intervals that separate interval j and interval k. For all but the smallest values of τ, the angles of particle displacements are effectively uncorrelated ($\langle\cos\theta_{jk}\rangle \approx 0$), except for consecutive time intervals ($k = j + 1$), where the motion is negatively correlated: $\langle\cos\theta_{j,j+1}\rangle < 0$. The magnitude of the negative correlation increases as the temperature is decreased.

Fig. 7 shows that, to a good approximation, we may simplify the sum over k in the second term of eq. (4) by setting all $\cos\theta_{jk}$ terms to 0 unless $k = j+1$. We then arrive at a corrected form of eq. (3).

$$\begin{aligned}
\langle\mathbf{r}_i(t,\tau)^2\rangle &= \left\langle \sum_{j=1}^{m} \left(\Delta\mathbf{r}_i(j)^2 + 2\Delta r_i(j)\Delta r_i(j+1)\cos\theta_{j,j+1}\right) \right\rangle \\
&= \left\langle \sum_{j=1}^{m} \Delta\mathbf{r}_i(j)^2 \right\rangle \times (1 + 2\langle\cos\theta_{j,j+1}\rangle). \qquad (5)
\end{aligned}$$

The second line assumes that the magnitudes of the displacement vectors for adjacent time

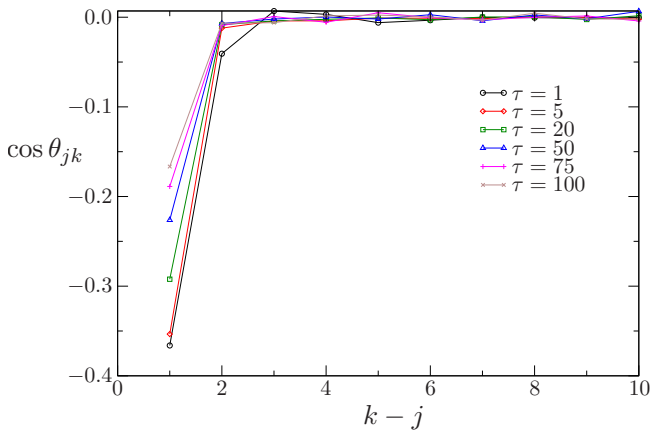

FIG. 7. Average correlation factor between displacements in time intervals of length τ, presented as a function of the time elapsed between the two intervals, $k - j$. θ_{jk} is the angle between the displacement vectors in interval j and interval k. All times are given in MD units, $t_{int} = 1.68\,\mathrm{ps}$. For all but the shortest interval lengths, $\cos\theta_{jk}$ decays very rapidly as a function of $j - k$ such that all intervals except for $k = j + 1$ may be considered uncorrelated. For $k = j + 1$ the correlation factor is negative, indicating that particle displacement vectors frequently reverse in consecutive time intervals.

intervals are similar when averaged over large m, so that $\Delta r_i(j+1) \approx \Delta r_i(j)$. The diffusion constant computed from this expression can be simplified to

$$D^*(T,\tau) = D(T,\tau)(1 + 2\langle\cos\theta_{j,j+1}\rangle). \tag{6}$$

The effect of including the correction term for OTP is shown in fig. 8. For all the values of τ considered, $D^*(T,\tau)$ is significantly closer to the true long-time $D(T)$ than the uncorrected $D(\tau)$. This result is true at all temperatures, so that super-Arrhenius behaviour is partially recovered when the correction factor is included, as expected from the BLJ study.[20] Using the correction factor, $D^*(T,\tau)$ agrees well with $D(T)$ for all $\tau > 250\,t_{\mathrm{int}}$. In contrast, the uncorrected $D(T,\tau)$ fails to reproduce $D(T)$ accurately in the low-temperature region, even for τ as large as $1000\,t_{\mathrm{int}}$.

These results show that accounting for negative correlation gives a good description of the observed super-Arrhenius behaviour. All particle displacements in OTP are negatively correlated over short time windows, so particles have a smaller net displacement than if motion were uncorrelated. The magnitude of the negative correlations increases as temperature decreases, leading to smaller diffusion constants and an apparent increase in the effective barrier to diffusion.

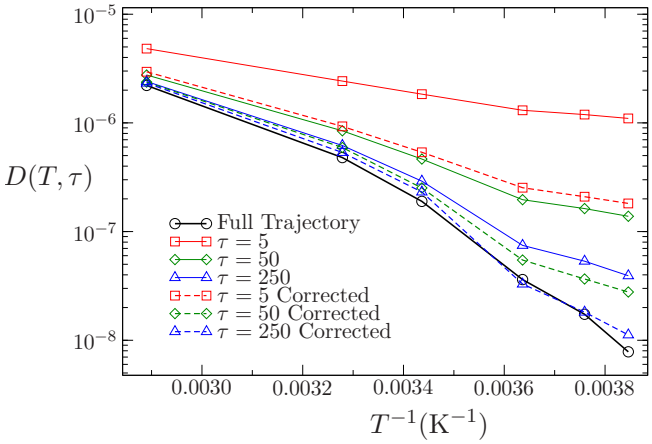

FIG. 8. Effective diffusion constants $D^*(T,\tau)$, incorporating a correction term computed from the average correlation factor for consecutive time intervals. Several values of the interval length τ are shown. Time is measured in internal MD units, $t_{int} = 1.68\,\mathrm{ps}$. The full-trajectory and uncorrected diffusion constants are shown for comparison. Including the correction term gives a dramatic improvement in agreement with the full-trajectory values, for all values of τ. Super-Arrhenius behaviour is retrieved at much lower values of τ than is observed for the uncorrected short-time diffusion constants.

To link these results with the cage-breaking description of diffusion we can attribute the negative correlation to a combination of cage rattling motion (non-cage-breaking rearrangements) and reversed CBs. The absence of super-Arrhenius curvature in the cage-breaking diffusion constants (fig. 5) therefore suggests that our method does not capture all of the unproductive, negatively correlated motion. We will investigate this further in the future.

The timescale analysis method is a coarse-graining approach, using progressively less information from the trajectory as τ is decreased. Cage-breaking diffusion constants can also be considered as a coarse-graining method, since any one molecule does not contribute to the effective diffusion constants for much of the trajectory. However, even for the coldest trajectory available the frequency of CBs is on the order of one per dimensionless time unit. In contrast, values of τ in excess of $1000\,t_{int}$ are required to give effective diffusion constants that fit the correct values as well as those obtained from CBs. So the cage-breaking method reproduces the diffusive behaviour in its region of validity with coarse-graining on a much shorter timescale than is required when using the arbitrary coarse-graining of the timescale method. This result suggests that the cage-breaking method is reasonably successful at identifying the important rearrangements which contribute to diffusion.

A. A more sophisticated intermolecular potential for OTP

The reduced timescale method is a very general approach that can indicate the importance of correlation effects in a system without requiring a practical method to identify which types of translational motion are important and productive.

Although accounting for the orientation of OTP molecules in the rigid Lewis-Wahnström model adds significantly to the complexity of the system relative to an atomic glass former such as BLJ, this model still neglects most of the important molecular degrees of freedom in OTP. The most important simplification is the replacement of the benzene rings by isotropic Lennard-Jones sites. In a more detailed model, we expect that using planar, rotatable rings will change the details of the mechanisms by which cage breaks occur. In particular, cage-breaking motions consisting of multiple elementary transitions may become important.

Eastwood *et al.* have proposed an atomistic model for OTP that includes nearly all the degrees of freedom.[26] We use a single trajectory at 290K produced for this model by the Shaw group, and compute the average correlation angle as in eq. (4). The behaviour of this angle as a function of time and τ is shown in fig. 9, and appears qualitatively identical to the results for the Lewis-Wahnström model (fig. 7). We therefore expect to observe similar behaviour in the short-time apparent diffusion constants; trajectories at other temperatures will be analysed in future work.

These preliminary results indicate that the anticorrelation effect still holds for the Shaw model of OTP, in which case we expect other aspects of its dynamical behaviour to reflect those of the Lewis-Wahnström model. In particular, we expect that the important rearrangements for translational diffusion will still be cage breaks, in the sense that they will involve changes of molecular nearest-neighbours and will mostly be discrete jumping events over reasonably large distances. However, the exact atomic mechanisms by which these cage breaks take place will be different in a more flexible model and so our definition for identifying them will require modification if it is to work with this more realistic system.

V. LANDSCAPE ANALYSIS

Two complementary descriptions of diffusion in supercooled OTP have now been presented. In the first, productive cage breaks were identified as the rearrangements that

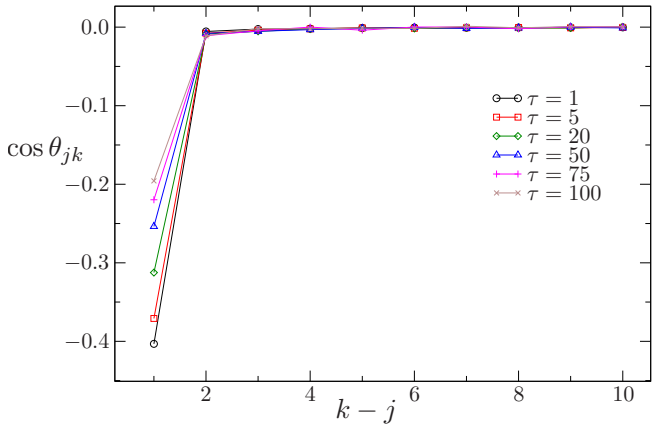

FIG. 9. Average correlation factor between displacements in time intervals of length τ using the Shaw group atomistic trajectory computed at 290K. Compare with fig. 7, which shows qualitatively the same behaviour. This suggests that the same conclusions regarding the importance of negative correlation will apply to this more sophisticated model as well as to Lewis-Wahnström OTP. Note that the MD time units used here, $t_0' = 200.02\,\mathrm{ps}$, are different from those in fig. 7.

contribute most to long-time diffusion in the moderately supercooled regime. In the second we showed that super-Arrhenius behaviour of the translational diffusion constants is caused by increasing negative correlation of particle displacements at lower temperatures, which arises partly from the types of motion excluded by the productive CB definition. In this section, we attempt to explain both of these aspects of the temperature-dependent dynamics by investigating the underlying potential energy landscape.

The potential energy landscape provides a powerful framework for interpreting and investigating thermodynamics and dynamics.[8,10,58,64–66] The PEL, $V(\mathbf{X})$, is defined as the potential energy expressed as a function of all system coordinates, $\mathbf{X}$. To simplify the analysis we consider a representative sample of the stationary points of V. In particular, we aim to sample local minima and saddle points with a Hessian index of one, which correspond to geometrical transition states (TSs).[67] These structures largely control the equilibrium and dynamic properties of the system.[3]

Following Goldstein[68] it is generally accepted that the dynamics of liquids at moderately supercooled temperatures depend strongly on the underlying PEL. The distribution of potential energy minima available to the system, and especially the heights of the energy barriers connecting them, are essential components of any microscopic description of diffusion and relaxation processes in supercooled liquids.[1] Direct sampling of both minima and

transition states should provide insight into the causes of the negative correlations described in the preceding sections.

A. Exploring the PEL

There are several approaches for sampling the landscape.[69–71] To study dynamics, it is important to explore the landscape in the same way as the model system. To this end, the inherent structure trajectories described in section III B were used to provide initial samples of local minima. Since these minima are derived from locally ergodic MD trajectories they should be representative of the configuration space explored by supercooled liquids.[70] The OPTIM program[72] was used to find pathways composed of minimum-TS-minimum triples that connect each pair of minima from the inherent trajectory. The resulting set of pathways contains a representative sample of stationary points across a wide region of the landscape. The PEL is temperature-independent, but this sampling method is not, so the landscape appears different when constructed from trajectories at different temperatures. We considered trajectories obtained at 291 K and 266 K, which correspond to the lower end of the landscape-influenced dynamical regime.[39] Consequently, the regions of the landscape sampled by these trajectories will be relevant to the supercooled dynamics of the system. The analysis of these two trajectories yielded qualitatively similar results and so, for brevity, only the results at 266 K are presented here.

OPTIM uses two algorithms to identify pathways connecting minima. An approximate initial pathway is determined by the doubly-nudged[73,74] elastic band[75,76] (DNEB) algorithm. The maxima on this pathway are candidate structures for transition states, which are refined by hybrid eigenvector-following[8,77,78] to obtain tightly converged transition states. Once a transition state has been found, the minima it connects are determined by perturbing the geometry slightly in opposite directions along the unique eigenvector corresponding to negative curvature, and then minimising (again using LBFGS)[59,60] to trace out an approximate minimum-energy pathway to the relevant potential minima. This procedure generates a minimum-TS-minimum triple for each TS. If the resulting triples do not form a connected pathway between the two initial minima, then the connection algorithm is applied again to a pair of intermediate minima selected using a modified Dijkstra algorithm.[79] This process is repeated until a complete pathway is found between the two original endpoints.

The Lewis-Wahnström OTP system is composed of rigid molecules, which require special treatment in landscape sampling methods. In OPTIM, they are described by a generalised coordinate system based on the angle-axis rotation formalism.[64,80–82]

B. Disconnectivity Graphs

Samples of minima and transition states can be visualised using disconnectivity graphs.[83,84] These graphs illustrate the energies of the minima and their connectivity through the transition states in the database. Interconversion between two minima at a particular threshold energy is possible if there exists a connected path between them that involves no transition state with potential energy higher than the threshold. This criterion allows all the minima to be grouped into mutually accessible subsets (superbasins)[83] at a given energy. As the threshold energy is decreased the subsets partition into smaller groups, until each contains a single minimum. The vertical axis of the disconnectivity graph corresponds to potential (or free) energy, and at each threshold energy every subset is represented by a single point, spaced along the horizontal axis for clarity. Each subset is connected by lines to its parent at the next higher threshold energy and to one or more daughter subsets at the next lower threshold (down to the level of individual minima, at which the line terminates).

The structure of the disconnectivity graph can provide insight into emergent properties of the landscape. Some systems show graphs that slope steeply down towards the global minimum, with low energy barriers connecting local minima to the main superbasin. This type of system will typically self-assemble to the global minimum very efficiently.[8,85] Glasses, in contrast, have highly frustrated landscapes where many minima with similar energies are separated by high barriers compared to relevant thermal energies. The minima span a wide range of energies, but there is no overall funnel and hence no specific structure-seeking behaviour. As the temperature of the liquid is decreased, and crossing any particular barrier becomes slower, the system becomes trapped on the experimental timescale behind the higher barriers in progressively smaller regions of the landscape. The glass transition corresponds to the system becoming localised in a small region containing relatively few local minima.[66]

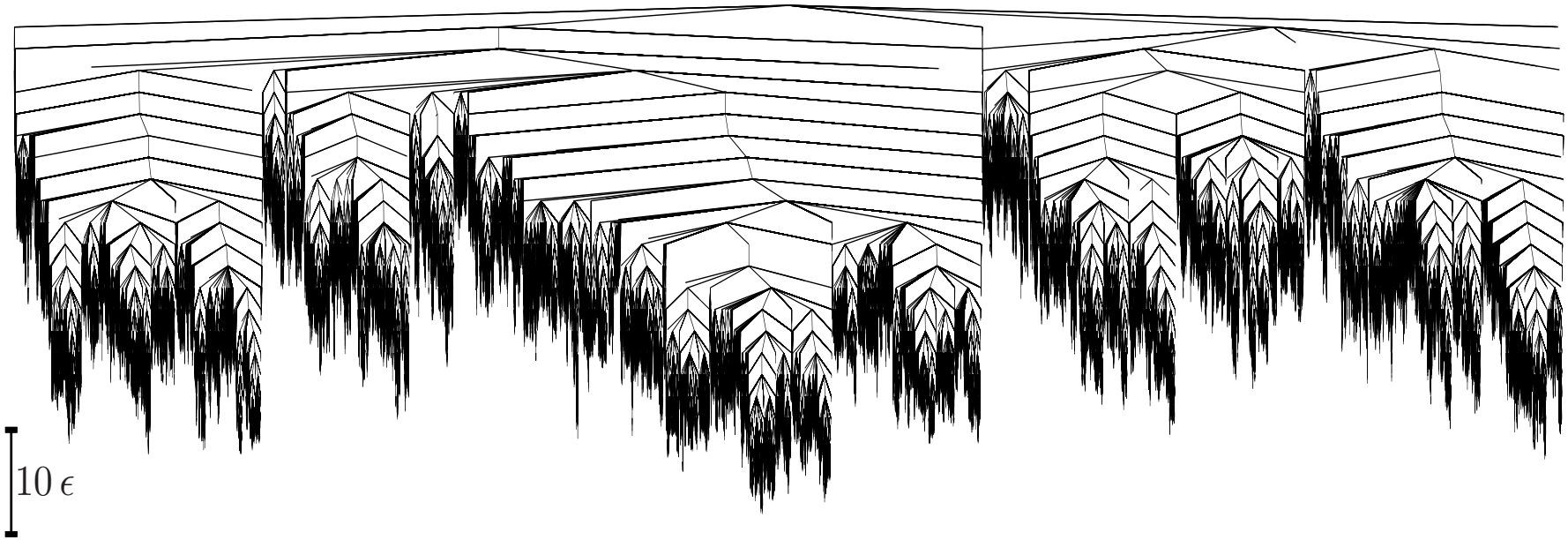

FIG. 10. Disconnectivity graph for OTP, produced by connecting each pair of adjacent minima in the inherent trajectory at 266 K. The potential energy landscape for OTP is highly frustrated and glassy.

Fig. 10 shows the disconnectivity graph of OTP obtained from the inherent trajectory at 266 K, well within the supercooled regime. The figure displays all the features of a glassy landscape described above: there is no clear global minimum, the energy barriers are large compared to k_BT, and there is no overall funnel structure. Although a low-energy region of the landscape corresponding to the crystal structure exists in principle, neither the real liquid nor the sampling algorithm finds this region on relevant time scales, instead exploring the many minima which correspond to amorphous configurations. There is a large range of barrier heights between the minima, many of which are much larger than k_BT in the supercooled regime.

The minima are clustered into many local groups within which they are separated by lower barriers (less than ϵ). The local groups can only interconvert by overcoming significantly larger barriers, so relaxation between them is comparatively slow. This organisation is consistent with the metabasin picture of glassy landscapes.[21,66,86] A metabasin may be defined as a set of minima that the system can traverse rapidly and reversibly. Transfer between metabasins is effectively irreversible, thus reducing diffusion to a random walk between metabasins. Intra-metabasin transitions are much more frequent than jumps between metabasins. It has been argued that the division of a glassy landscape into metabasins is sufficient to produce super-Arrhenius behaviour.[66] This suggestion is compatible with the description based on negatively correlated displacements (section IV), since these correlations arise from reversed transitions within a metabasin.

Metabasin transitions have been associated with abrupt changes in the energy of the minima visited by an inherent trajectory.[86] However, the hierarchical structure seemingly apparent within the landscape of OTP suggests that it may be possible to identify a microscopic definition that divides the landscape into a series of local funnels, which behave like metabasins according to the energy-based definition. Since it has been recognised that productive (i.e. non-reversed) CBs may be a good alternative definition of metabasins, in the following section we investigate the effect of partitioning the landscape into cage-breaking and non-cage-breaking transitions.

C. Cage-breaking Analysis of the Landscape

The cage-breaking analysis described in section III may be applied to any pair of configurations of the system, including two minima connected by a transition state. If any molecular cage breaks occur between these two minima, the minimum-TS-minimum triple is classified as cage-breaking. Otherwise, it is classified as non-cage-breaking.

Fig. 11 shows a disconnectivity graph for OTP from which all non-cage-breaking transition states have been removed. This transformation causes the disconnectivity graph to fragment wherever a removed transition state provided the only connection between two sets of minima. Each fragment is then coloured according to the energy at which it becomes disconnected from the rest of the graph, to show visually the connectivity of this transformed landscape. Minima which are only connected to the rest of the landscape by non-cage-breaking transitions are omitted entirely from the disconnectivity graph, but these account for a small proportion of the total number of minima.

Fig. 11 shows that most of the landscape belongs to a small number of connected regions, each appearing as a large block of a single colour in the graph. This result shows that the removal of non-cage-breaking transition states does not significantly break the connectivity of the landscape: cage breaks according to our definition are largely sufficient to describe the connectivity. The fact that the graph does partially disconnect when non-cage-breaking transitions are removed does not necessarily mean that some non-cage-breaking transitions are essential to explore the entire landscape. The sampling method described in section V A is not intended to identify every possible pathway between a given pair of minima. So where two fragments become disconnected in fig. 11, there may well be other pathways connecting these fragments by cage-breaking transition states only, which have not been located. Since there are only a small number of significant fragments in fig. 11, it is likely that only a few additional cage-breaking transition states would need to be located to connect the entire landscape.

Fig. 12 is produced in the same way as fig. 11, but with all the cage-breaking transition states removed instead of the non-cage-breaking transition states. In contrast to the CB-only graph, fig. 12 is highly fragmented into many small unconnected regions, many containing only a few minima at similar energies. A CB is required to cross between two such regions.

Some of the alternative pathways that have not been detected by the sampling method

will connect pairs of minima by sequences of non-cage-breaking transitions only. Including these would increase the connectivity of fig. 12, but because there are so many missing connections it seems unlikely that the landscape would ever become globally connected without the inclusion of CBs. This result reinforces the earlier conclusion that cage-breaking rearrangements are an essential component of diffusion, since diffusion requires traversing the landscape, which is impossible without CBs.

As shown in fig. 13, the non-CB-only graph shows small locally connected regions of the landscape, which can be crossed without needing a CB transition. This figure suggests hierarchical ordering of the landscape into a set of local funnels, separated by the requirement for a cage-breaking transition to move between them.

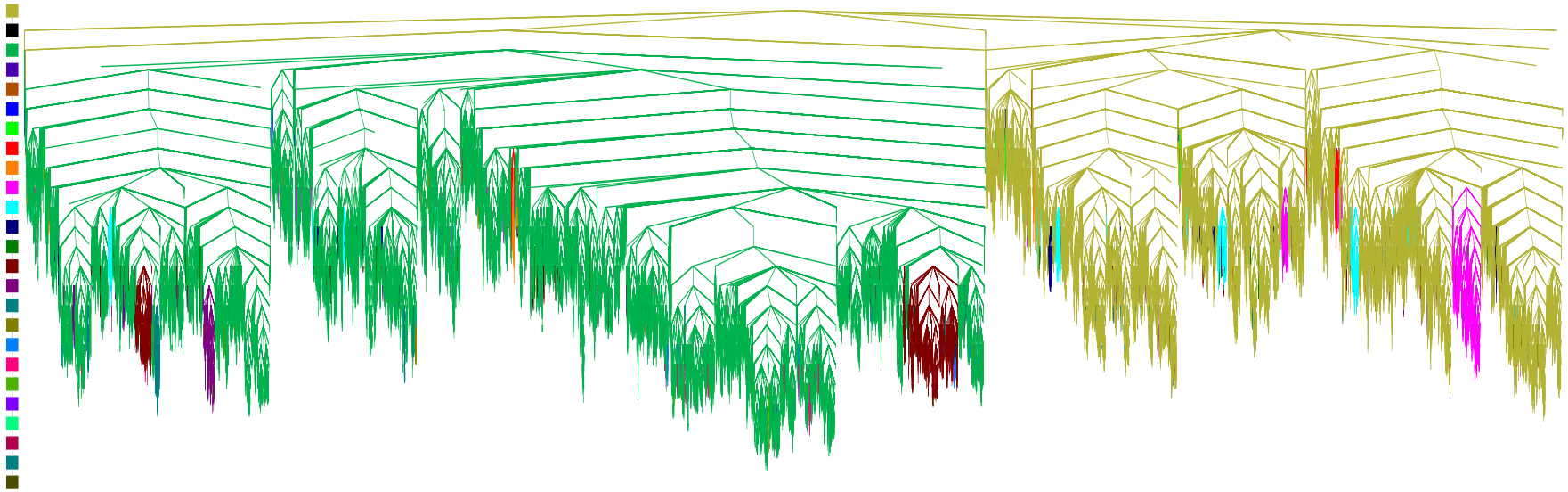

FIG. 11. Disconnectivity graph based on fig. 10 but removing all non-cage-breaking transition states. Some groups of minima are only connected to the rest of the database by non-cage-breaking transition states, so in this figure they appear disconnected from the rest of the landscape. These fragments are coloured according to the energy level at which they become disconnected, as shown by the scale bar at the left. The separation of energy levels is $2\,\epsilon$. The graph is almost completely connected, suggesting that non-cage-breaking transitions are not essential to explore the entire landscape.

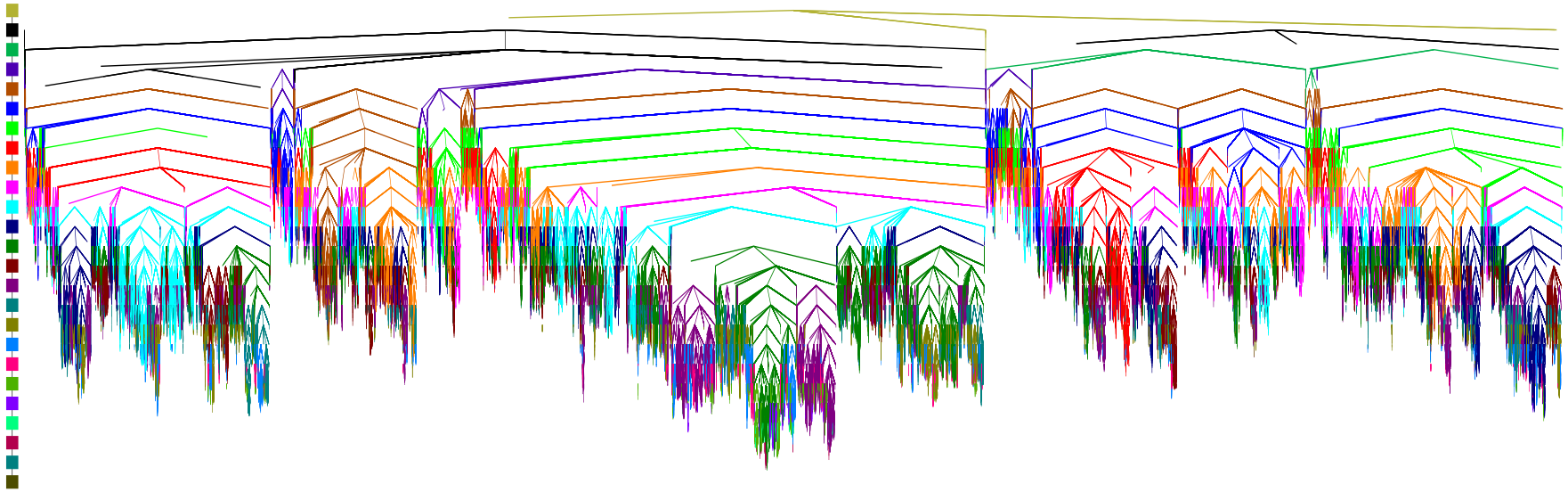

FIG. 12. As fig. 11 but in this case all non-cage-breaking transition states are retained and all cage-breaking transition states are removed. The graph is highly fragmented compared to fig. 11, demonstrating that it is impossible to explore the supercooled region of the landscape without undergoing cage-breaking transitions.

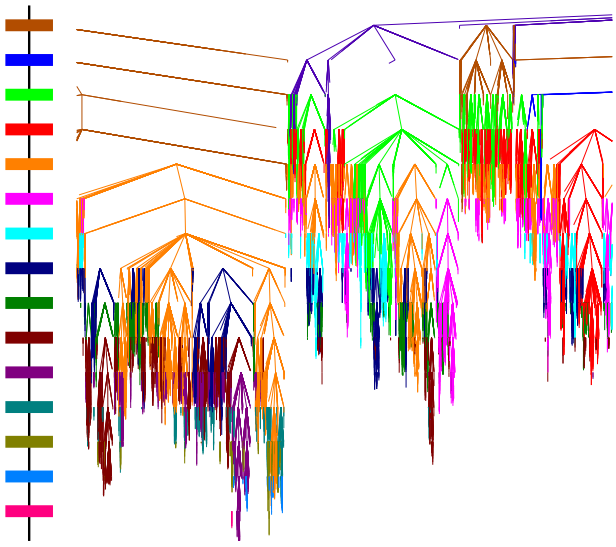

FIG. 13. Detail from fig. 12 showing local connectivity in the non-cage-breaking landscape. The scale bar and colouring scheme are the same as for fig. 12.

It seems likely that the local funnels in fig. 12 can be identified with groups of minima each contained within a metabasin.[58] To investigate this proposition we must establish whether transitions between these minima are easily reversible, as expected. We estimate the reversibility of transitions between the minima of our database by constructing a connected path from the inherent trajectory used in section V A by replacing each pair of minima in the trajectory by the shortest pathway of minimum-TS-minimum triples between them. Because the inherent trajectory frequently revisits regions of configuration space, this process reintroduces time-dependent behaviour, including reversals in particle motion, into the landscape database.

Every pair of minima on the connected path was analysed for CBs and reversals. Following the BLJ study,[21] we defined a "metabasin transition" as taking place every time a productive CB occurred (see section III B). Fig. 14 shows the landscape with all productive CBs removed, and demonstrates that this definition partitions the landscape into completely connected local funnels, which become disconnected from each other at higher energies. Fig. 15 shows a detail from this graph corresponding to the same region of the landscape as fig. 13, for comparison. Note the greatly increased connectivity within a funnel once reversed CBs are taken into account.

The hierarchical structure observed by considering CBs without dynamical information

is preserved when that information is included. Because the gaps between connected regions in fig. 14 are accessed by non-reversed transitions, we expect diffusion at low temperatures to approximate a random walk between these connected funnels. This is the justification for describing the funnels as microscopically defined metabasins. However, investigations into the correspondence of productive CBs with energy metabasin (EMB) transitions[10,86] are ongoing, which will help to assess the validity of this description.

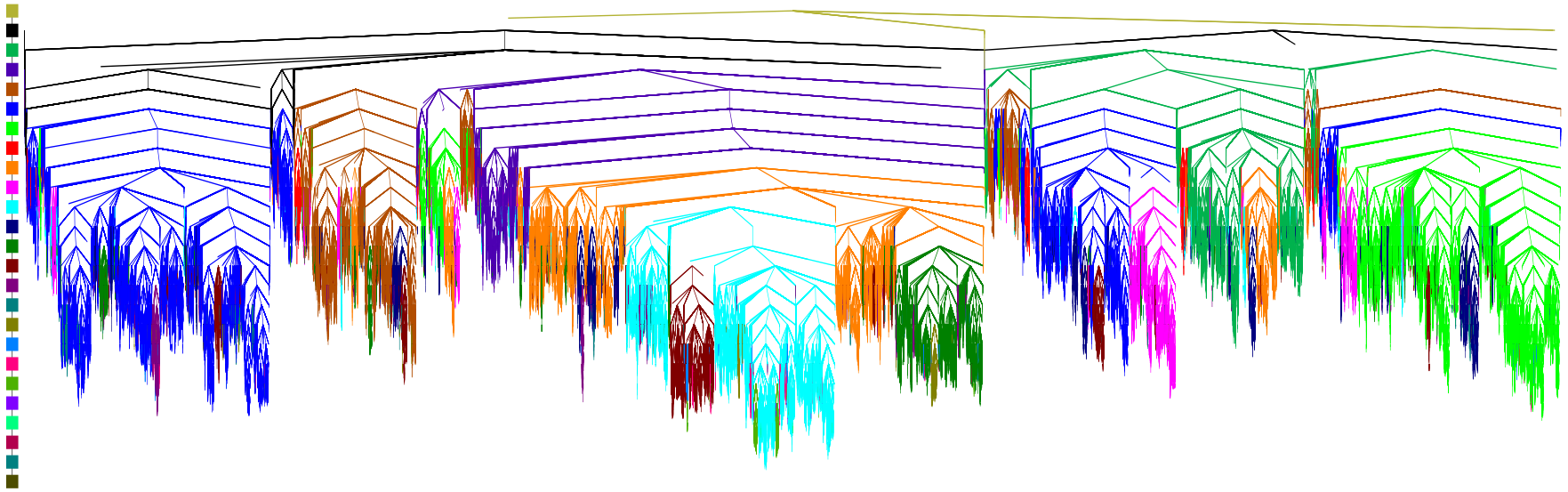

FIG. 14. Disconnectivity graph for OTP at 266 K after removing all transition states corresponding to productive CBs as identified by a connected path analysis (see text). Disconnected fragments of the graph are coloured according to the energy level at which they become disconnected from the rest of the graph, as shown by the scale bar at the left. The separation of energy levels is $2\,\epsilon$. The landscape is partitioned into a hierarchy of superstructures. Transition between superstructures requires a non-reversed (productive) CB, so movement between superstructures should approximate a random walk, which suggests that they may correspond to metabasins.

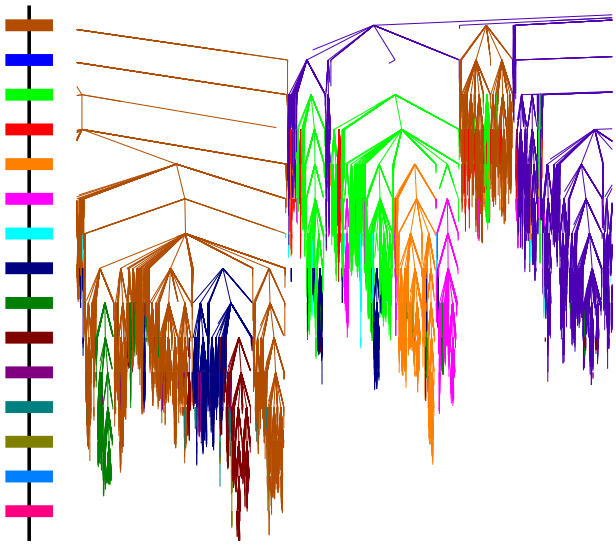

FIG. 15. Detail from fig. 14 showing increased local connectivity compared to fig. 13 now that transition states corresponding to reversed cage breaks are included. The connected regions in this detail possibly correspond to individual metabasins. The scale bar and colouring scheme are the same as for fig. 14.

VI. CONCLUSIONS

There are three important results to be taken from this computational study of supercooled Lewis-Wahnström ortho-terphenyl. First, that a greatly simplified, but still accurate, description of translational diffusion at moderately supercooled temperatures may be achieved using a microscopic definition of productive cage-breaking processes. Second, the super-Arrhenius temperature dependence of the translational diffusion constants in OTP results from increased negative correlations in displacements at low temperatures, and these correlations largely result from the reversed- and non- cage-breaking motion omitted from the productive cage-breaking picture. Third, the potential energy landscape for this molecular glass former may be divided into a discrete set of funnels, probably identifiable as metabasins, and these funnels can be distinguished by the requirement that transitions between them involve cage-breaking.

These conclusions are consistent with previous results for the bulk BLJ fluid,[19–22] which demonstrates that our analysis applies beyond the case of a simple atomic liquid. A coherent, simplified picture of diffusion in moderately supercooled fragile glass formers has now been

presented, directly referencing features of the underlying PEL.

A geometrical definition of a nearest-neighbour cage has been presented, which captures essential features of the PEL and of molecular dynamics. Our definition extends the scheme proposed for BLJ[21] to treat simple molecules. Moreover, two of the three system-dependent parameters required in the original definition have been removed, providing a much more general description of a cage-breaking transition. The new definition is in principle applicable to any glass former, although its validity for other systems remains to be confirmed. A more sophisticated system that could be investigated is the atomistic model of OTP proposed by Eastwood *et al.* (see section IV A).

We use a timescale analysis method to show that super-Arrhenius behaviour of the translational diffusion constants arises from increasingly negative correlations in particle motion at lower temperature. The types of motion which are excluded from our definition of productive cage-breaks, namely cage rattling and reversed cage-breaks, contribute to these negative correlations. The fact that the productive cage-break method is less successful at reproducing diffusion constants at lower temperature implies that our current method does not identify all reversals and negatively correlated rearrangements. If this aspect of the analysis can be improved, and super-Arrhenius behaviour retrieved from the cage-breaking method, we will be able to identify the reduced-timescale picture as containing a signature of cage-breaking processes, allowing the diffusion behaviour to be explained without needing to identify cage breaks microscopically.

Finally, the relationship of cage breaks and reversals to the potential energy landscape was explored. We have shown that it is impossible to explore the PEL in a locally ergodic fashion without undergoing cage-breaking transitions, which emphasises the importance of this type of rearrangement for long-time diffusion. By removing all productive cage-breaking transition states from our databse, we decompose the PEL into a set of connected funnels between which the system should move in a random-walk-like fashion. The funnels identified in this way probably correspond to metabasins.[58] We have therefore proposed a microscopic criterion, which reveals hierarchical order in the PEL of OTP.

Our results are consistent with a view of cooperative motion in OTP that is divided into more and less mobile regions. The more mobile molecules at any given time are the ones currently undergoing cage breaks, the less mobile are confined within their cages. It would be interesting to probe the extent of these regions and the exact nature of cooperative

movements, perhaps by looking for time and spatial correlations in the identified cage breaks. If a concrete connection can be found between the negative correlation and cage-breaking descriptions of diffusion, it probably lies in identification of the timescale for cage-breaking motion to occur, and the relationship between this timescale and the reduced timescale of the short-time apparent diffusion constants. Arriving at a clear statement of the relationship between these two pictures is an important challenge for future work.

Another future objective will be to compare our definition of cage-breaks with other methods for identifying important structural changes,[49,56,57] particularly those based on metabasins,[10,86,87] to understand whether they are capturing the same features of supercooled dynamics as cage breaks, and how these different definitions coincide with established theories of the glass transition. In particular, it would be interesting to see how much of the utility of the cage-breaking method comes from its non-local character, and whether the rearrangements picked out by other approaches have similar or different effects on the connectivity of the landscape.

The influence of the rotational degrees of freedom for OTP upon the results presented in this paper could also be investigated further by looking for a correlation effect in rotational diffusion analogous to that for translational diffusion described in section IV. Analysing this effect could help to explain super-Arrhenius behaviour of rotational diffusion constants, and possibly give new insights into the causes of low-temperature decoupling between translational and rotational diffusion constants in OTP.[24,33] Barriers to rotational transitions are smaller than those for translation, so reversals in motion are likely to be less frequent. However, it might be possible to define a geometrical motion analogous to the translational cage break that may help to describe the rotational fine structure on the PEL. The presence of cage-breaking transitions with low energy barriers, as seen in the disconnectivity graphs of section V C, hints at the importance of rotation to describe the fine details of the energy landscape.

ACKNOWLEDGMENTS

This work was supported by the University of Cambridge through a CHSS studentship to S.P.N., and by the ERC. The authors would like to thank D.E. Shaw Research for kindly providing us with the data used in section IV A. The program used to identify

cage breaks may be found on the Cambridge Energy Landscape Database, http://www-wales.ch.cam.ac.uk/CCD.html

REFERENCES

[1]Debenedetti, P.G. and Stillinger, F.H., *Nature*, **410**, 259 (2001)

[2]Cammarota, C. and Biroli, G., *Proc. Natl. Acad. Sci. USA*, **109**, 8850 (2012)

[3]Ediger, M.D. and Harrowell, P., *J. Chem. Phys.*, **137**, 080901 (2012)

[4]Kob, W., *J. Phys. Cond. Mat.*, **11**, R85 (1999)

[5]Angell, C.A., *Chem. Rev.*, **102**, 26272650 (2002)

[6]Lubchenko, V. and Wolynes, P.G., *Ann. Rev. Phys. Chem.*, **58**, 235 (2007)

[7]Stillinger, F.H. and Debenedetti, P.G., *Ann. Rev. Cond. Mat. Phys.*, **4**, 263 (2013)

[8]Wales, D.J., *Energy Landscapes*, (Cambridge University Press, Cambridge, 2003)

[9]Greer, A.L., *Science*, **267**, 1947 (1995)

[10]Doliwa, B. and Heuer, A., *Phys. Rev. E*, **67**, 031506 (2003)

[11]Ferrer, M.L., Lawrence, C., Demirjian, B.G., Kivelson, D., Albasimionesco, C. and Tarjus, G., *J. Chem. Phys.*, **109**, 8010 (1998)

[12]Elmatad, Y.S., Chandler, D. and Garrahan, J.P., *J. Phys. Chem. B*, **113**, 5563 (2009)

[13]Mallamace, F., Branca, C., Corsaro, C., Leone, N., Spooren, J., Chen, S.H. and Stanley, H.E., *Proc. Nat. Acad. Sci. USA*, **107**, 22457 (2010)

[14]Mallamace, F., Corsaro, C., Stanley, H.E. and Chen, S.H., *Eur. Phys. J. E*, **34**, 94 (2011)

[15]Chen, Z., Angell, C.A. and Richert, R., *Eur. Phys. J. E*, **35**, 65 (2012)

[16]Zhao, J., Simon, S. and McKenna, G.B., *Nature Communications*, **4**, 1783 (2013)

[17]Angell, C.A., *Science*, **267**, 1924 (1995)

[18]de Souza, V.K. and Wales, D.J., *J. Chem. Phys.*, **123**, 134504 (2005)

[19]de Souza, V.K. and Wales, D.J., *Phys. Rev. B.*, **74**, 134202 (2006)

[20]de Souza, V.K. and Wales, D.J., *Phys. Rev. Lett.*, **96**, 057802 (2006)

[21]de Souza, V.K. and Wales, D.J., *J. Chem. Phys.*, **129**, 164507 (2008)

[22]de Souza, V.K. and Wales, D.J., *J. Chem. Phys.*, **130**, 194508 (2009)

[23]Cicerone, M.T., Blackburn, F.R. and Ediger, M.D., *J. Chem. Phys.*, **102**, 471 (1995)

[24]Mapes, M.K., Swallen, S.F. and Ediger, M.D., *J. Phys. Chem. B*, **110**, 507 (2006)

[25]Mallamace, F., Corsaro, C., Leone, N., Villari, V., Micali, N. and Chen, S.H., *Sci. Rep.*,

4, 3747 (2014)

[26]Eastwood, M.P., Chitra, T., Jumper, J.M., Palmo, K., Pan, A.C. and Shaw, D.E., *J. Phys. Chem. B*, **117**, 12898 (2013)

[27]Kudchadkar, S.R. and Wiest, J.M., *J. Chem. Phys.*, **103**, 8566 (1995)

[28]Mossa, S., Di Leonardo, R., Ruocco, G. and Sampoli, M., *Phys. Rev. E*, **62**, 612 (2000)

[29]Ghosh, J. and Faller, R., *Mater. Res. Soc. Symp. Proc.*, **924**, 0924 (2006)

[30]Mossa, S., Ruocco, G. and Sampoli, M., *Phys. Rev. E*, **64**, 021511 (2001)

[31]Lewis, L.J. and Wahnström, G., *Phys. Rev. E*, **50**, 3865 (1994)

[32]Mossa, S., Nave, E.L., Stanley, H.E., Donati, C., Sciortino, F. and Tartaglia, P., *Phys. Rev. E*, **65**, 041205 (2002)

[33]Lombardo, T.G., Debenedetti, P.G. and Stillinger, F.H., *J. Chem. Phys.*, **125**, 174507 (2006)

[34]Rinaldi, A., Sciortino, F. and Tartaglia, P., *Phys. Rev. E*, **63**, 061210 (2001)

[35]Stoddard, S.D. and Ford, J., *Phys. Rev. A*, **8**, 1504 (1973)

[36]Okumura, H., Itoh, S.G. and Okamoto, Y., *J. Chem. Phys.*, **126**, 084103 (2007)

[37]Thirumalai, D., Mountain, R.D. and Kirkpatrick, T.R., *Phys. Rev. A*, **39**, 3563 (1989)

[38]Rahman, A., *Phys. Rev.*, **136**, A405 (1964)

[39]Sastry, S., Debenedetti, P.G. and Stillinger, F.H., *Nature*, **393**, 554 (1998)

[40]Pedersen, U.R., Hudson, T.S. and Harrowell, P., *J. Chem. Phys.*, **134**, 114501 (2011)

[41]Kob, W. and Andersen, H., *Phys. Rev. E*, **51**, 4626 (1995)

[42]Doliwa, B. and Heuer, A., *Phys. Rev. Lett.*, **80**, 4915 (1998)

[43]Doliwa, B. and Heuer, A., *Journal of Physics: Condensed Matter*, **11**, A277 (1999)

[44]Weeks, E.R. and Weitz, D.A., *Phys. Rev. Lett.*, **89**, 095704 (2002)

[45]Weeks, E.R. and Weitz, D., *Chemical Physics*, **284**, 361 (2002)

[46]Götze, W. and Sjögren, L., *J. Phys. C.*, **21**, 3407 (1988)

[47]Fujara, F., Geil, B., Sillescu, H. and Fleischer, G., *Z. Phys. B*, **88**, 195 (1992)

[48]Chaudhuri, P., Berthier, L. and Kob, W., *Phys. Rev. Lett.*, **99**, 060604 (2007)

[49]Pastore, R., Coniglio, A. and Pica Ciamarra, M., *Soft Matter*, **10**, 5724 (2014)

[50]Middleton, T.F. and Wales, D.J., *Phys. Rev. B*, **64**, 024205 (2001)

[51]Rabani, E., Gezelter, J.D. and Berne, B.J., *J. Chem. Phys.*, **107**, 6867 (1997)

[52]Rabani, E., Gezelter, J.D. and Berne, B.J., *Phys. Rev. Lett.*, **82**, 3649 (1999)

[53]Rabani, E., Gezelter, J.D. and Berne, B.J., *J. Chem. Phys.*, **110**, 3444 (1999)

[54]Rabani, E., Gezelter, J.D. and Berne, B.J., *Phys. Rev. Lett.*, **85**, 467 (2000)

[55]Candelier, R., Widmer-Cooper, A., Kummerfeld, J.K., Dauchot, O., Biroli, G., Harrowell, P. and Reichman, D.R., *Phys. Rev. Lett.*, **105**, 135702 (2010)

[56]Vollmayr-Lee, K., *J. Chem. Phys.*, **121**, 4781 (2004)

[57]Kluge, M. and Schober, H.R., *Phys. Rev. B*, **70**, 224209 (2004)

[58]Heuer, A., *J. Phys. Cond. Mat.*, **20**, 373101 (2008)

[59]Nocedal, J., *Mathematics of Computation*, **35**, 773 (1980)

[60]Liu, D. and Nocedal, J., *Math. Prog.*, **45**, 503 (1989)

[61]Chill, S.T., Stevenson, J., Ruehle, V., Shang, C., Xiao, P., Farrell, J.D., Wales, D.J. and Henkelman, G., *J. Chem. Theor. Comput.*, **10**, 5476 (2014)

[62]van Meel, J.A., Filion, L., Valeriani, C. and Frenkel, D., *J. Chem. Phys.*, **136**, 234107 (2012)

[63]Chong, S.H. and Kob, W., *Phys. Rev. Lett.*, **102**, 025702 (2009)

[64]Wales, D.J., *Phil. Trans. Roy. Soc. A*, **363**, 357 (2005)

[65]Wales, D.J., *Phil. Trans. Roy. Soc. A*, **370**, 2877 (2012)

[66]Stillinger, F.H., *Science*, **267**, 1935 (1995)

[67]Murrell, J.N. and Laidler, K.J., *Trans. Faraday Soc.*, **64**, 371 (1968)

[68]Goldstein, M., *J. Chem. Phys.*, **51**, 3728 (1969)

[69]Kirkpatrick, S., Gelatt, C.D. and Vecchi, M.P., *Science*, **220**, 671 (1983)

[70]Stillinger, F.H. and Weber, T.A., *Science*, **225**, 983 (1984)

[71]Wales, D.J. and Doye, J.P.K., *J. Phys. Chem. A*, **101**, 5111 (1997)

[72]Wales, D.J., OPTIM: A program for characterising stationary points and reaction pathways, http://www-wales.ch.cam.ac.uk/OPTIM/

[73]Trygubenko, S.A. and Wales, D.J., *J. Chem. Phys.*, **120**, 2082 (2004)

[74]Sheppard, D., Terrell, R. and Henkelman, G., *J. Chem. Phys.*, **128**, 134106 (2008)

[75]Henkelman, G., Uberuaga, B.P. and Jónsson, H., *J. Chem. Phys.*, **113**, 9901 (2000)

[76]Henkelman, G. and Jónsson, H., *J. Chem. Phys.*, **113**, 9978 (2000)

[77]Munro, L.J. and Wales, D.J., *Phys. Rev. B*, **59**, 3969 (1999)

[78]Zeng, Y., Xiao, P. and Henkelman, G., *J. Chem. Phys.*, **140**, 044115 (2014)

[79]Carr, J.M., Trygubenko, S.A. and Wales, D.J., *J. Chem. Phys.*, **122**, 234903 (2005)

[80]Kusumaatmaja, H., Whittleston, C.S. and Wales, D.J., *J. Chem. Theor. Comput.*, **8**, 5159 (2012)

[81]Rühle, V., Kusumaatmaja, H., Chakrabarti, D. and Wales, D.J., *J. Chem. Theor. Comput.*, **9**, 4026 (2013)

[82]Chakrabarti, D., Kusumaatmaja, H., Ruhle, V. and Wales, D.J., *Phys. Chem. Chem. Phys.*, **16**, 5014 (2014)

[83]Becker, O.M. and Karplus, M., *J. Chem. Phys.*, **106**, 1495 (1997)

[84]Wales, D.J., Miller, M.A. and Walsh, T.R., *Nature*, **394**, 758 (1998)

[85]Wales, D.J., Doye, J.P.K., Miller, M.A., Mortenson, P.N. and Walsh, T.R., *Adv. Chem. Phys.*, **115**, 1 (2000)

[86]Doliwa, B. and Heuer, A., *Phys. Rev. E*, **67**, 030501(R) (2003)

[87]Cao, P., Li, M., Heugle, R.J., Park, H.S. and Lin, X., *Phys. Rev. E*, **86**, 016710 (2012)